buildings

MDPI

Article

Strength Design of Ultra-High-Performance Fiber-Reinforced Cementitious Composites Using Local Ecological Admixture

Rui Ma [1], Xun Hu [1], Huiying Hu [1], Ziyang Tian [1], Lei Chen [2] and Jinyu Zong [2,*]

[1] Anhui Province Engineering Laboratory of Advanced Building Materials, Anhui Jianzhu University, Hefei 230601, China
[2] Anhui Sanjian Engineering Co., Ltd., Hefei 230001, China
* Correspondence: englishyuzi@126.com

Abstract: The ultra-high-performance fiber-reinforced cementitious composite (UHPFRC) is a new generation of building material with extremely high mechanical strength and durability, which can be used for ultra-high, thin-wall or long-span construction, that prolongs the service life of construction in severe environments. In this study, UHPFRC was prepared with a high range of local ecological admixture to decrease the material's cost and the environmental impact. Raw materials' proportions, water/binder ratio, fiber-volume contents, and hybrid-fiber ratio were studied on the property improvement of UHPFRC, and an F-test analysis was induced to reveal the important significance on compressive strength. The results demonstrated that the compressive strength of 237.8 MPa was achieved with mineral admixture substitution over 40%. The particle-packing density and the binder reactivity both succeeded on the compressive strength. Water/binder ratio determined the hydration degree and the flowability of UHPFRC, which affected compressive strength through hydration products and microstructure. Also, compressive strength was more sensitive with hybrid-fiber than fiber-volume content. The order of importance for compressive strength was powder proportion > hybrid-fiber ratio > fiber-volume content > water/binder ratio.

Keywords: strength design; UHPFRC; high-range local admixture; compressive strength; significance analysis

Citation: Ma, R.; Hu, X.; Hu, H.; Tian, Z.; Chen, L.; Zong, J. Strength Design of Ultra-High-Performance Fiber-Reinforced Cementitious Composites Using Local Ecological Admixture. *Buildings* **2022**, *12*, 2230. https://doi.org/10.3390/buildings12122230

Academic Editors: Ahmed Senouci and Elena Ferretti

Received: 22 November 2022
Accepted: 12 December 2022
Published: 15 December 2022

1. Introduction

With the fast developing of urbanization in decades, high performance and long service life are becoming the primary acquirements for construction materials due to the growing demands and the environmental friendship development [1–5]. Ultra-high-performance fiber-reinforced cementitious composite (UHPFRC) is an advanced construction material with super-high mechanical properties and durability [6–11]. The compressive strength of UHPFRC is commonly higher than 150 MPa, and the permeability is suggested to be 5–10 times lower than normal concrete as well [12,13]. So far, UHPFRC plays an increasingly important role in several fields, such as infrastructure construction, super engineering, and structural repairment [14–17], to improve the performance and prolong the service life. However, a large fraction of high-activity binders and fine powders were necessary in UHPFRC to guarantee the performance [18–22]. For example, cement dosage usually ranged from 900 to 1100 kg/m^3 in UHPFRC [20,23,24]. High cement demand caused a series of problems, including exceeded consumption of natural resources, large CO_2 emissions, high hydration heat, large volume shrinkage, and expensive material costs [11,25–27]. Hence, industrial by-products and solid wastes were attempted to substitute cement or quartz sand to decrease the environmental impacts and materials costs [25,28–34], and even some also presented positive effects on shrinkage deformation and corrosion resistance of UHPFRC [35,36].

Ultra-high strength is the most important advantage of UHPFRC that caused both engineering and economic benefits [37]. High strength offered sufficient possible constructions on engineering design and structural evolution [38,39]. UHPFRC was preferred for some super projects for enough structural stability and service life [40], for instance, the river-cross bridge with main span larger than 1 km. High strength UHPFRC also matched better with the high strength steel rebar than normal concrete. In addition, ultra-high strength declined with the usage of construction materials per volume, making buildings lighter, thinner, and lower cost [41]. To achieve the ultra-high strength, high amounts of fine active binders and autoclave curing were commonly induced [42], while the substitution of cement with mineral admixtures was against the strength development. Ali Sadrmomtazi [21] found that with an increase of silica fume replacement, the compressive strength decreased both at 7 and 28 days. According to references, the compressive strength of UHPC was mostly less than 200 MPa when substituted with mineral admixtures and without autoclave curing [20,25,26,29,35]. Unfortunately, using substitutable materials and the non-autoclave method to prepare UHPFRC with compressive strength over 200 MPa is still a challenge.

UHPFRC is a complex and expensive mixture, and its performance far varies with the raw-materials proportion and curing regime. Although several standards were proposed by regions and organizations recent years, it was still hard to achieve a formulary approach for UHPFRC preparation. Moreover, to reduce the cost and environmental impact, ternary or quaternary active industrial by-products and solid wastes were often selected as supplementary cementitious materials (SCMs) to substitute cement or aggregates in UHPFRC [30–32,43–46]. Yang et al. [35] used phosphorous slag to induce a low-carbon design of UHPFRCC, and the compressive strength slightly decreased even with 50 wt% of cement substituted by slag, and the autogenous shrinkage was reduced by 45.6% from the maximum. Li et al. [36] developed quaternary blends, including cement, ground-granulated blast-furnace slag (GGBS), limestone powder (LP), and microsilica, to evaluate the properties of UHPFRC. A sustainability efficiency of 130% was reached, with the decrease of CO_2 about 59%. However, the properties of these ternary/quaternary blends of UHPFRC were far different due to their materials' categories and mix proportions. So far, the performance for UHPFRC products mostly depended on a series of experimental tests rather than theoretical predication. Some researchers studied the design procedures of UHPFRCC [47,48]. Shi et al. [11] considered the cost and CO_2 emission during UHPC preparation and calculated the compressive strength and embodied CO_2 index to design the UHPC with low environment impact. Arora et al. [20] studied the effect of matrix and fiber volume on the mechanical strength and predicted the compressive and flexural strength through the digital-image-correlation method.

In this work, UHPFRC with compressive strength exceeding 200 MPa was designed with a high volume of SCMs and non-pressed curing method, and the strength development factors and the influence efficiency were also studied to guide the proportion design. Fly ash and silica fume as SCMs and local river sand as aggregates were applied to conduct the degree of environmental impact. The effects of the materials' aspects, including binder proportion, water-to-binder ratio, steel–fiber content, and hybrid-fiber ratio, on workability and strength development were investigated. To evaluate the significance of each variable on strength development, an F-test based on ANOVA(Analysis of Variance) was induced. The calculation of F follows from Equation (1) [49]:

$$F = \frac{SS_a/f_a}{SS_e/f_e} \quad (1)$$

where SS_a is the sum of squared deviations of factors, f_a is the freedom degree of factors, SS_e is the sum of squared deviation for experimental error, and f_e is the freedom degree for SS_e. The higher F value indicates that the corresponded factor was more significant for strength development. The results could be used to guide the materials' mix proportions for UHPFRC and helpful for strength adjustment if necessary.

2. Materials and Methods

2.1. Raw Materials and Mix Proportion

The binder materials used in this study were P·I 52.5 Portland cement according to Chinese standard and class F fly ash (FA) and silica fume (SF) from a local powder plant as mineral admixture. The chemical composition and critical physical properties of binders are listed in Table 1. Local river sand with a fineness modulus of 2.4 and maximum grain size of 2.36 mm was utilized as fine aggregate. The particle-size dispersion of raw powder materials is present in Figure 1. High-range polycarboxylate-superplasticizer powder was carried to afford an available flowability of cementitious mixture. Two fibers with different geometry, straight steel fiber (SSF) and end-hooked steel fiber (HSF), were used to reinforce the mechanical properties of UHPFRC. The physical index of fibers is listed in Table 2. To reveal the effect of the materials' proportions on UHPFRC with high strength, powder gradation (M16B1, M16B2, and M16V0), water-to-binder ratio (W/B, M14V1, M15V1, M16V1, and M17V1), fiber content (M16V0, M16V1, and M16V2), and hybrid-mixed ratio (M16V1, M16H1, M16H2, M16H3, M16H4, and M16H5) were varied and the influences on workability and mechanical development were investigated. In experiments, the value for each variable was determined based on our previous work [33,34,50,51] for powder gradation, where PC:FA:SF:Sand = 5:4:1:12, 6:3:1:12, and 6:3:1:10, respectively. W/B ranged from 0.14–0.17, volumes fraction of steel fiber were 1.5%, 2.0%, and 2.5%, and the ratios of SSF:HSF = 1:0, 4:1, 3:1, 2:1, 1:1, and 0:1, respectively. The details of mix proportion are listed in Table 3.

Table 1. Chemical compositions and physical properties of binders.

		PC	FA	SF
Chemical composition (%)				
CaO		64.47	7.68	1.68
Al_2O_3		4.87	26.88	0.32
Fe_2O_3		3.59	5.19	0.05
SiO_2		20.87	53.25	95.06
MgO		2.13	2.26	0.39
SO_3		2.52	0.92	0.55
N_2O		0.11	0.70	0.11
K_2O		0.65	1.14	0.38
L.O.L		0.77	1.02	0.68
Physical properties				
Specific gravity		3.3	2.3	2.3
Specific surface area (m^2/kg)		369	–	20,000
Standard consistency (%)		27.4	–	–
Initial setting time (min)		127	–	–
Final setting time (min)		182	–	–
Flexural strength (MPa)	3 d	7.3	–	–
	28 d	10.6	–	–
Compressive strength (MPa)	3 d	38.0		
	28 d	65.8		

Table 2. Physical indices of steel fibers used in the experiment.

Type	Length (L)/mm	Equivalent Diameter (D)/mm	L/D Radio	Tensile Strength/MPa
Straight steel fiber	13	0.2	65	2000
End-hooked steel fiber	14	0.2	70	2000

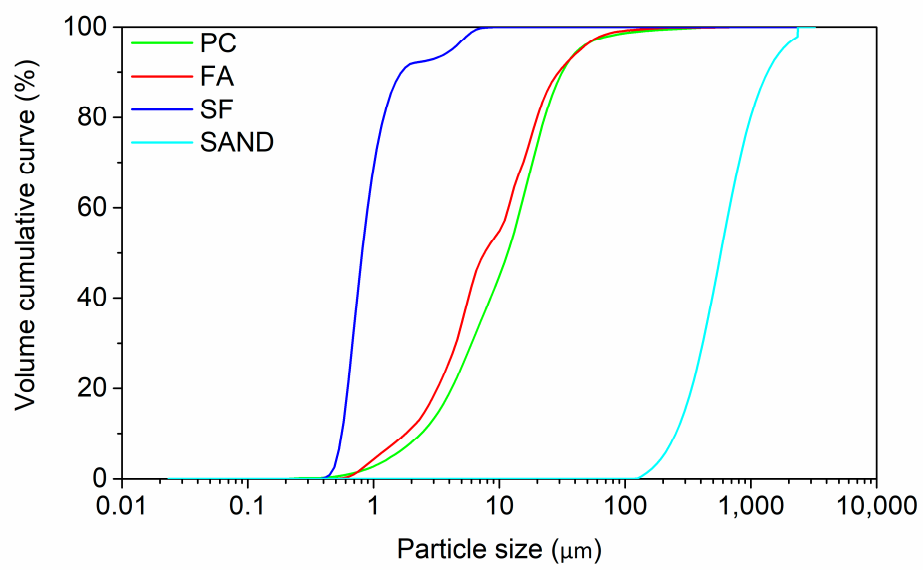

Figure 1. Particle-size distribution of raw materials.

Table 3. Mix-proportion details of ecological UHPFRCC (kg/m^3).

	PC	FA	SF	Sand	Water	SSF	HSF	SP
M16B1	480	384	96	1150	153.6	158	–	16.9
M16B2	583	291	97	1166	155.4	158	–	17.1
M16V0	632	316	105	1053	168.5	158	–	17.6
M14V1	643	322	107	1072	150	198	–	17.1
M15V1	636	318	106	1060	158.9	198	–	17.0
M16V1	629	324	105	1048	167.6	198	–	16.8
M17V1	622	311	104	1036	176.1	198	–	16.6
M16V2	625	313	104	1042	166.7	237	–	16.7
M16H1	629	324	105	1048	167.6	158	40	16.8
M16H2	629	324	105	1048	167.6	149	49	16.8
M16H3	629	324	105	1048	167.6	132	66	16.8
M16H4	629	324	105	1048	167.6	99	99	16.8
M16H5	629	324	105	1048	167.6	–	198	16.8

In order to avoid the disruption from sand and steel fibers, some paste samples with the same mix proportion but without sand and steel fiber were also prepared for XRD and TG tests.

2.2. Mix Procedure

Due to low W/B, a reversed mix procedure was adopted to maximize the dispersion effect of polycarboxylate superplasticizer. Powder materials, including binders, sand, and superplasticizer, were first stirred together at low speed for 1 min to mix well. After that, all powders were added into water under low-speed stirring for 5–8 min until a uniform mortar was formed; then high-speed stirring was applied for another 1 min to achieve an available flowability. At last, the steel fibers were mixed and stirred for 2–3 min for thorough dispersion. The fresh UHPFRC mixture was casted and placed under standard conditions (20 ± 2 °C, RH ≥ 95%) for 48 h until demolded, then was steam curried at 85 °C for designed age.

2.3. Test Methods

2.3.1. Particle-Size Distribution

The particle-size distribution of binder materials was measured by a laser particle-size analyzer (LPSA), and ethanol was selected as solvent to avoid hydrated reaction. An amount of 5 g powder was measured and ultrasonic dispersed in 100 mL of ethanol for 3 min; then the mixed solution was dropped into the sample chamber of the equipment until enough of the amount formed. For each sample, the test was repeated twice, and we calculated the results for the average.

Since the particle size of sand was mostly beyond the measuring range of the LPSA, the curve of sand-size distribution was fitted from the grading curve.

2.3.2. Flowability of Fresh UHPFRC

The flowability of UHPFRC was evaluated following Chinese standard (GB/T 2419-2005). The fresh matrix was first filled into a cone-shaped mold on a platform of a jolting table. Then the mold was vertically removed and switched on the table in time. After jolting 25 times, two perpendicular diameters were measured, and the mean value was record as the flowability.

2.3.3. Mechanical Strength

The flexural and compressive strengths were measured according to the standard BS EN 196-1. Three prism specimens with the size of 40 mm × 40 mm × 160 mm were prepared for each mix proportion. The flexural strength was determined by three-point bending with the upload rating of 2.4 kN/s, the ultimate strength for each prism specimen was recorded, and the average value was calculated. Then, six broken ends after flexure testing were used for axial compression tests, and the average value of maximum strength was used as the final compressive strength.

2.3.4. Hydration Products

The crystalline structure and the content of hydration products were investigated by X-ray diffraction (XRD) and thermal gravimetric analysis (TG). After steam curing at 85 °C for the designed age, the paste samples were stopped of hydration by alcohol and grinded into powder to pass through the 80 μm sieve. During XRD testing, the sample was scanned from 5° to 90° (2θ) at the rate of 0.15 s/step, with the step of 0.02° (2θ). During TG testing, the sample was ignited from 25 °C to 1000 °C, with the rate of 10 °C/min under nitrogen atmosphere.

2.3.5. Morphology

A scanning electron microscope (SEM) was used to observe the morphology of paste samples by the backscattered electronic (BSE) mode, with the operating voltage of 15 kV. For sample preparation, the paste fragments were first stopped of hydration at the designed age and dried at 40 °C in a vacuum oven for 48 h, then were impregnated by epoxy under vacuum at 40 °C for 48 h until hardened. After that, the samples were polished by sand paper to the roughness of 0.1 μm. Finally, carbon film was coated on the sample surface to avoid charging during the experiment.

3. Results and Discussion

3.1. Raw-Materials Proportion

Based on the MAA model [43], the optimal packing grading curve was calculated from Equation (2) and is presented in Figure 2 as the target curve. The actual integral grading curves from the series of materials' proportions are also compared in Figure 2. The

diversion between the target curve and actual curves is evaluated by the determination coefficients (R^2) and listed in Table 4.

$$P(D) = \frac{D^q - D^q_{min}}{D^q_{max} - D^q_{min}} \quad (2)$$

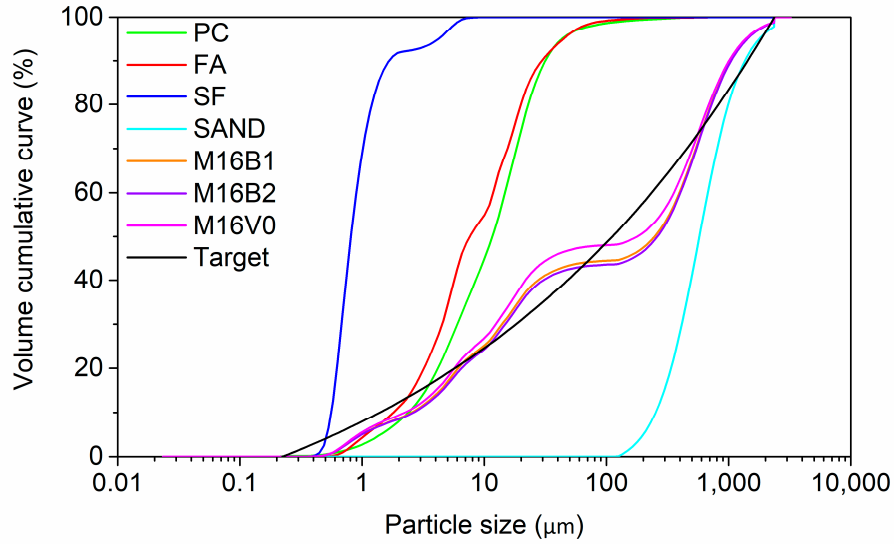

Figure 2. Particle-size distribution of the ingredients, showing target and experimental grading curves.

Table 4. The determination coefficients of experimental and target curves.

	Determination Coefficient (R^2)
M16B1	0.9762
M16B2	0.9772
M16V0	0.9688

The actual particle-packing curves for different powder proportions are also shown in Figure 2. It is seen that the actual curves are not perfectly fitting with the target one. Compared with the target curves, more of a fraction of the large-sized particles over 500 μm existed, and more particles smaller than 10 μm were still preferred. The determination coefficients, which are listed in Table 4, were all beyond 0.9. Notably, the sample M16B2, composed with the proportions of PC:FA:SF = 6:3:1, as well as the binder-to-sand ratio of 1:1.2, presented the most-closed grading curve to the target one, and supposedly had the densest packing proportion.

The flexural and compressive strengths of samples with different material proportion were also tested, and the results are shown in Figure 3.

In Figure 3, the strength of the densest packing of M16B2 was higher than that of M16B1, but less than that of sample M16V0, which contained the highest weight percentage of cement. The results implied that the packing density was beneficial to strength development, but the synergistic effect of packing density and cement dosage resulted in the best strength performance.

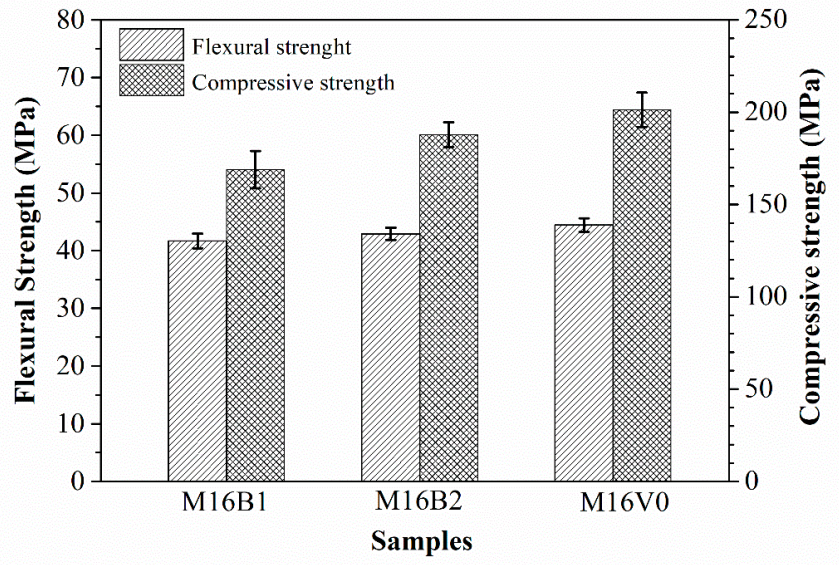

Figure 3. Flexural and compressive strengths of samples with different proportions.

3.2. Water-to-Binder Ratio

Water was necessary to supply available flowability and promote the hydration reaction of UHPFRC. To investigate the effect of water on strength development, the water-to-binder ratio (W/B) for samples was varied from 0.14 to 0.17, keeping the other parameters constant. Once the W/B was 0.14, the fresh matrix was too dry to cast, and when the W/B increased to 0.17, the flowability of the fresh sample much improved, where even a water film formed on the matrix surface, as seen in Figure 4. The flowability of samples almost linearly increased from 167.5 mm to 280.0 mm with increasing W/B, as seen in Figure 5. It is well accepted that more water leads to better fluidity. However, the viscosity of fresh UHPFRCC also changed significantly with different W/B ratios and will be studied in further work.

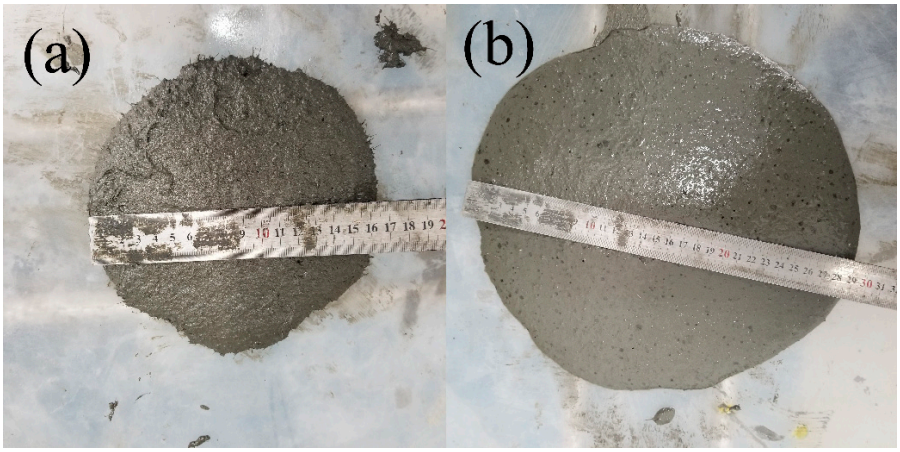

Figure 4. The test picture of fresh samples with the W/B ratios of 0.14 and 0.17. (**a**) W/B = 0.14 (**b**) W/B = 0.17.

The strength development with different W/B ratios is revealed in Figure 6. The compressive strengths of samples were all over 180 MPa, with a maximum of 216 MPa. It is usually known that lower W/B ratios are positive for strength development. However, in this research, with the W/B increasing, the compressive strength was first increased to the maximum at W/B = 0.16, then decreased again, and the flexural strength was decreased about 12.6% with the incremental W/B ratio.

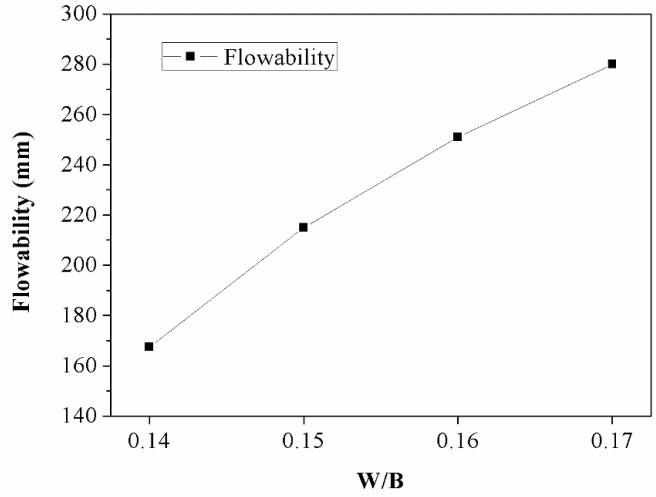

Figure 5. Flowability of fresh samples with different W/B ratios.

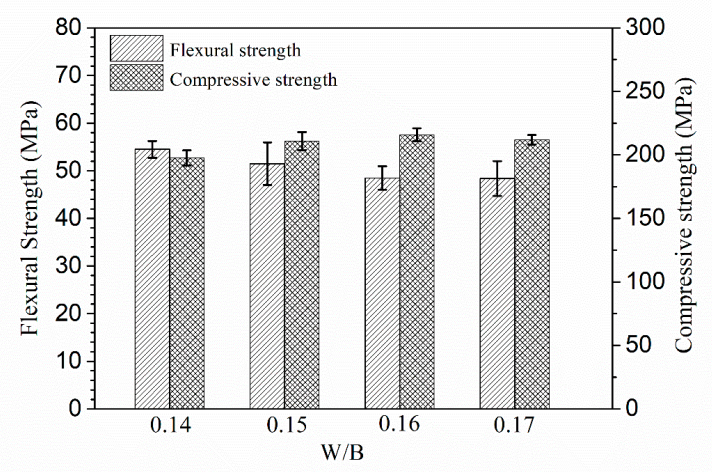

Figure 6. Flexural and compressive strengths of UHPFRCC with different W/B.

UHPFRC can be defined as the hardened cementitious composites formed by unreacted binder and aggregates bonded with hydration gel, where the gel content is important to immobilize the skeleton. Since cement was not fully reacted in UHPFRC, the dosage of hydration gel was increased with the raised W/B ratio, leading to a better bonding property. On the other hand, the strength of gel was lower than aggregates and unreacted binder, so the extensive gel caused worse strength performance. Proper gel content is vital for strength improvement. To examine this inference, the hydration degree and the hydration-product content were analyzed by TG and SEM.

The TG curves for samples are presented in Figure 7. There were several mass-loss steps that corresponded to the thermal reaction of the composites with water vapor or CO_2 released during the heating process. The weight loss below 105 °C could be attributed to the evaporation of free water and interlayer water from C-S-H. The mass loss between 105 °C and 410 °C was due to the dehydration of hydration products, including C-S-H, ettringite, and AFm. The reactions at 410–640 °C and 640–800 °C were due to the decompositions of $Ca(OH)_2$ and $CaCO_3$, respectively [52]. The step at the temperatures between 800 °C and 900 °C was possibly caused by the phase transformation from α_H' C_2S to α_L' C_2S.

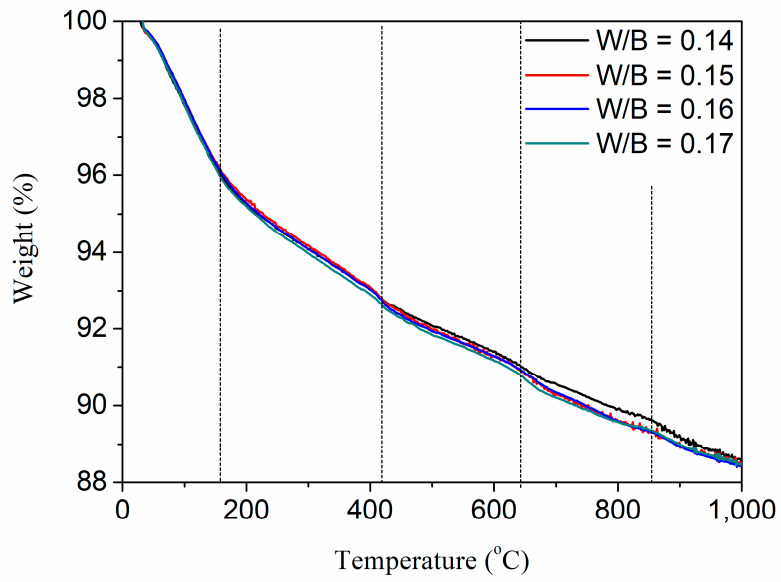

Figure 7. TG curves for samples with W/B = 0.14 to 0.17.

Since the $CaCO_3$ in samples was mostly generated from the carbonation of $Ca(OH)_2$, the content of $Ca(OH)_2$ and non-evaporated water can be calculated from Equations (3) and (4):

$$W_C = 74/18 \cdot Ldx + 74/44 \cdot Ldc \quad (3)$$

$$W_n = Ldh + Ldx + 18/44 \cdot Ldc \quad (4)$$

where W_C and W_n are the contents of $Ca(OH)_2$ and non-evaporated water in the sample, respectively. Ldh, Ldx, and Ldc are the relative mass losses on the TG curve due to the dehydration of C-S-H and ettringite, the dehydroxylation of $Ca(OH)_2$, and the decarbonation of $CaCO_3$, respectively. According to Equations (2) and (3), the content variation of $Ca(OH)_2$ and the relative hydration degree compared to M14V1 were calculated and are shown in Figure 8. The CH content was increased to W/B = 0.15, then decreased, and the relative hydration degree reached the maximum when W/B = 0.16.

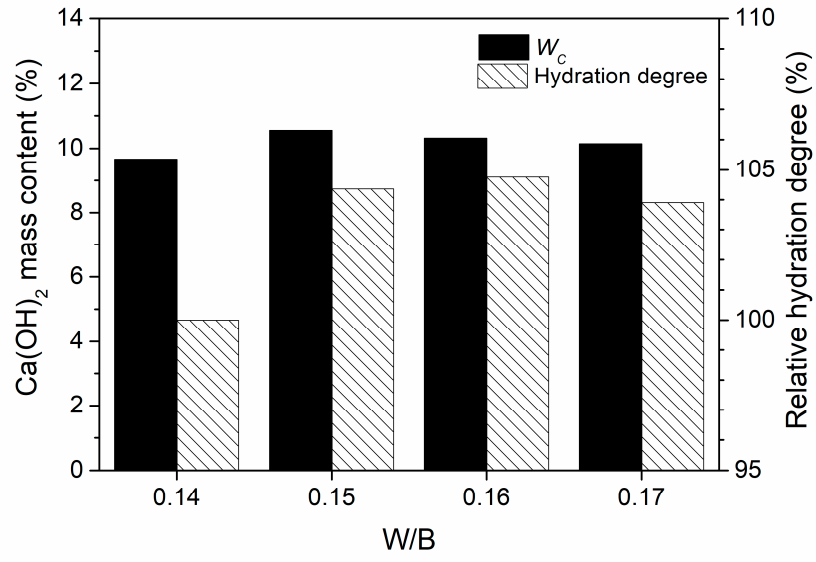

Figure 8. The $Ca(OH)_2$ content and relative hydration degree with W/B from 0.14 to 0.17.

It is well understood that more water promoted the hydration reaction of cement particles. However, the relative hydration degree decreased when W/B = 0.17 in this research.

Combined with the flowability results, it is assumed that the mortar at W/B = 0.17 was too moist so that part of water evaporated from the surface quickly after casting, causing a lower hydration degree. This result was also confirmed according to the strength test.

Moreover, compared between samples M15V1 and M16V1, although the hydration degree of M16V1 was higher, the content of CH was less than that of M15V1. This revealed that the pozzolanic reaction in M16V1 was more intensive and consumed more CH, and more secondary hydration gel was generated, which is also good for compressive strength.

The BSE images for UHPFRC with different W/B are also shown in Figure 9. The bright irregular particles were unreacted cement, and the round particles were FA. The marked hydration products in Figure 9 were the following: 1—inner C-S-H, 2—C-S-H from FA hydrated, 3—out C-S-H. From Figure 9, it is clear that unreacted cement and FA particles were surrounded by uniform C-S-H gel. However, with the W/B increased, more broken cement particles with blurry boundaries were found in Figure 9d, which implies that the hydration degree increased.

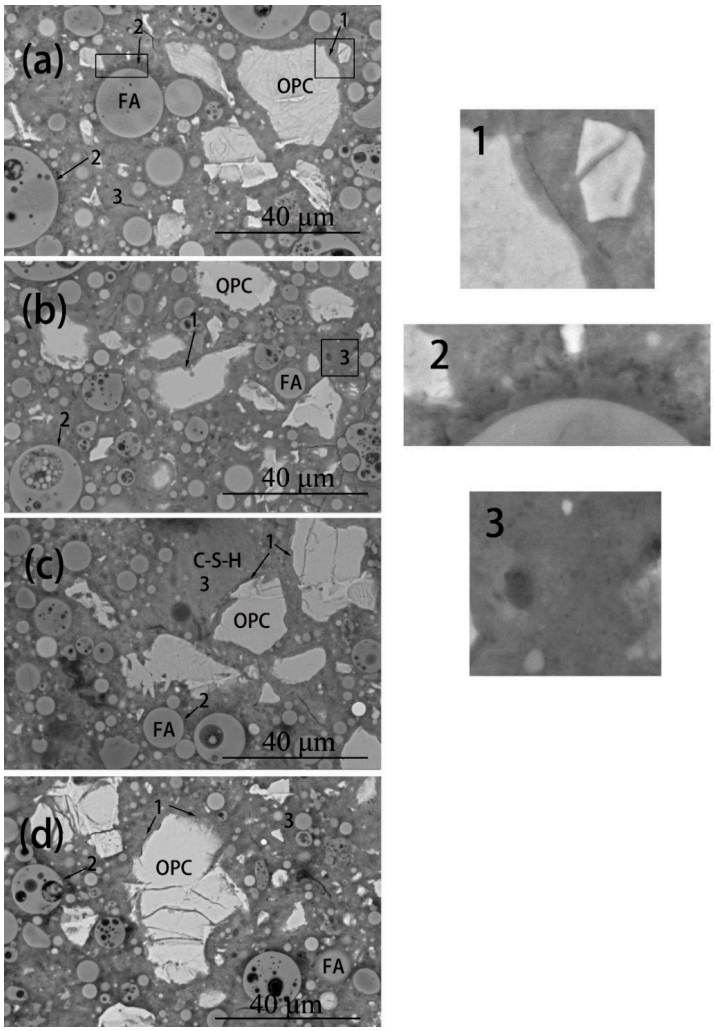

Figure 9. BSE images for UHPFRC with W/B of (**a**) 0.14, (**b**) 0.15, (**c**) 0.16, (**d**) 0.17.

3.3. Fiber Content and Fiber Geometry

The fracture of UHPFRC specimens during strength testing was caused by the unstable propagation of cracks, while fibers exhibit outstanding resistance on crack formation and propagation due to the bridge effect. In our previous work, the pull-out energy of fibers with different geometry and the flexural strength of hybrid-reinforced UHPFRC were discussed in [34]. The ability of fibers for crack control was dominated by fiber geometry, fiber content,

and fiber hybrid. The strength development of UHPFRCC varied with fiber-volume content and hybrid-steel–fiber ratio, which are presented in Figures 10 and 11, respectively.

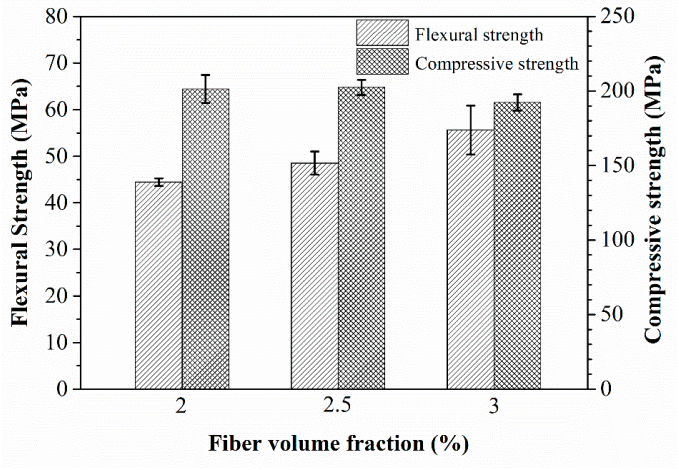

Figure 10. The strengths of UHPFRCC with different fiber contents.

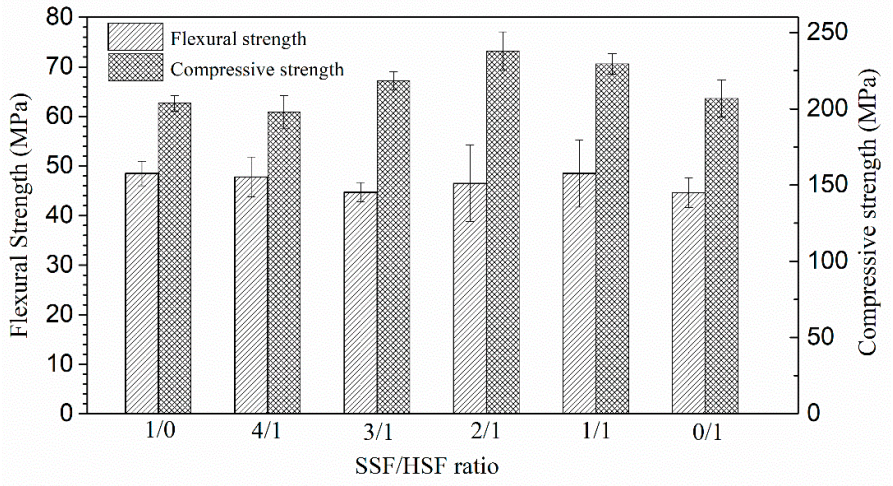

Figure 11. The strengths of UHPFCC with different hybrid-fiber ratios.

In Figure 10, the compressive strength and flexural strength, respectively, of UHPFRC were 201.3 and 44.4, 202.4 and 48.5, and 192.3 and 55.6 MPa, with the steel–fiber volume fractions of 2%, 2.5%, and 3%, respectively. Moreover, as the HSF/SSF ratio increased from 0% to 100%, the compressive strength first increased from 203.7 MPa to a maximum of 237.8 MPa, then decreased to 206.8 MPa again, while flexural strength changed slightly around (46.5 ± 2) MPa, as shown in Figure 11.

The results implied that the compressive strength was not sensitive for steel–fiber content, and when the fiber exceeded the amount used, the strength decreased due to more initial defects. While HSF was beneficial for compressive-strength development, the strength increased with more HSF in the available range. However, the flexural strength performed opposite to the compressive strength. The flexural strength increased with the raised usage of steel fiber, and the increased range was about 25% when the steel–fiber-volume fraction increased from 2% to 3%. As the fiber volume remained constant, the flexural strength vibrated in a narrow range.

The essential fact of compressive or flexural fracture is the through-crack formed under stress, and the fiber improves strength by resisting the crack extension due to the bridge effect. Under flexural stress, a large crack formed in the bending area, and the crack-resistance property of steel–fiber was more dependent on the friction during the pull-out process. The higher fiber-volume fraction increased with the resisted fiber amount.

However, in compressive cases, the crack width was much smaller than the former, so the anchoring effect worked significantly on crack resistance. Since HSF performed with higher adhesion strength, the compressive strength increased with the raised ratio of HSF/SSF. However, exceeded fiber content or HSF ratio also brought distribution problems, which were harmful for strength development.

3.4. The Effect Efficiency Index F

From the above results and discussions, the UHPFRC with local SCMs achieved 237.8 MPa after 7 days of steam curing. However, the compressive strength varied significantly with different material proportions. To reveal the dominant factor for strength design, the importance index of different material aspects was evaluated by the F-value.

The significance of powder packing, W/B ratio, steel–fiber content, and hybrid-fiber ratio on strength development was evaluated by the efficiency index F, and the value for each aspect was calculated according to Equation (1) and is listed in Table 5.

Table 5. The significance analysis of various variables using the F-test.

Independent Variable	SS_a	F_a	SS_e	F_e	F Value	Evaluation of Significance
Powder proportion	2850.7	2	759.0	15	28.2	Most significant
W/B	876.8	3	2198.8	20	2.7	Least significant
Fiber content	1369.1	2	689.9	14	13.9	Less significant
Fiber geometry	6445.6	5	2133.4	29	17.5	Significant

It is generally accepted that W/B ratio is the key factor for the ultimate strength of UHPFRC, and the lower W/B ratio refers to the higher strength. However, from this research, the compressive strength was more sensitive with powder packing than the fiber geometry. The higher strength of UHPFRC was contributed from the less initial defect and strong bonding strength between components. The dense packing powders helped to construct a compact skeleton for UHPFRC, and less C-S-H gel was needed to bind particles and fill pores. In practical application, the particle-size distribution of the component and the component proportion should be carefully selected for ultra-high-strength UHPFRC design. The W/B ratio affected the rheological properties of fresh mortar and the hydration degree, as well as the pore volume and pore structure, whose influence on strength was indefinite and should be cautiously experimented on in practical applications.

4. Conclusions

In this research, FA, SF, and river sand from local areas were used as substitution materials to design ecological UHPFRC, and the effect of materials for strength development was investigated. The importance of factors on strength was evaluated by the F-value of the ANOVA method. The following conclusions can be drawn:

(1) With a high range of substitution materials, the compressive strength of UHPFRC was beyond 180 MPa, and the maximum strength reached 237.8 MPa after 7 days of steam curing.
(2) The powder proportion played the key role in strength development. The strength increased with the synergetic effect of compact packing and high activity of binders.
(3) The fiber content was more efficient for flexural strength. Additionally, the compressive strength was more sensitively with the ratio of HSF, which performed well with high adhesion strength. However, the massive usage of fiber and HSF brought distribution problems that decreased the compressive strength.
(4) The W/B ratio ranged from 0.14 to 0.17 and was hesitated for use with compressive strength in practical applications. High W/B ratio was preferred to improve the flowability and increase the hydration degree but also induced more pores and cracks when water was consumed.

(5) The significance of different materials' aspects on compressive strength was evaluated by the F-value with the ANOVA method, and powder proportion was most important in the strength design of UHPFRC.

Author Contributions: Conceptualization, R.M.; methodology, X.H. and H.H.; formal analysis, X.H. and H.H.; investigation, J.Z.; resources, R.M.; writing—original draft preparation, R.M. and Z.T.; writing—review and editing, J.Z.; project administration, L.C.; funding acquisition, R.M. and L.C. All authors have read and agreed to the published version of the manuscript.

Funding: This work was supported by the National Natural Science Foundation (52208227), Ph.D. initial funding of Anhui Jianzhu University (2019QDZ15), Natural Science Research Key Project of Anhui Educational Committee (KJ2021A0625), Director Foundation of Anhui Province Engineering Laboratory of Advanced Building Materials (JZCL012ZZ), State Key Laboratory of Silicate Materials for Architectures (Wuhan University of Technology) (SYSJJ2022-18), and the research funding of Anhui Sanjian Engineering Co., Ltd. (RD2022-08).

Conflicts of Interest: The authors declare no conflict of interest.

References

1. Al Nuaimi, N.; Sohail, M.G.; Hawileh, R.A.; Abdalla, J.A.; Douier, K. Durability of reinforced concrete beams strengthened by galvanized steel mesh-epoxy systems under harsh environmental conditions. *Compos. Struct.* **2020**, *249*, 112547. [CrossRef]
2. Liu, Y.; Zhang, Z.; Shi, C.; Zhu, D.; Li, N.; Deng, Y. Development of ultra-high performance geopolymer concrete (UHPGC): Influence of steel fiber on mechanical properties. *Cem. Concr. Compos.* **2020**, *112*, 103670. [CrossRef]
3. Mhaya, A.M.; Huseien, G.F.; Abidin, A.R.Z.; Ismail, M. Long-term mechanical and durable properties of waste tires rubber crumbs replaced GBFS modified concretes. *Constr. Build. Mater.* **2020**, *256*, 119505. [CrossRef]
4. Nguyen, Q.D.; Castel, A. Reinforcement corrosion in limestone flash calcined clay cement-based concrete. *Cem. Concr. Res.* **2020**, *132*, 106051. [CrossRef]
5. Yoo, D.-Y.; Shin, W.; Chun, B.; Banthia, N. Assessment of steel fiber corrosion in self-healed ultra-high-performance fiber-reinforced concrete and its effect on tensile performance. *Cem. Concr. Res.* **2020**, *133*, 106091. [CrossRef]
6. Li, P.; Sluijsmans, M.; Brouwers, H.; Yu, Q. Functionally graded ultra-high performance cementitious composite with enhanced impact properties. *Compos. Part B Eng.* **2020**, *183*, 107680. [CrossRef]
7. Lee, J.-Y.; Yuan, T.; Shin, H.-O.; Yoon, Y.-S. Strategic use of steel fibers and stirrups on enhancing impact resistance of ultra-high-performance fiber-reinforced concrete beams. *Cem. Concr. Compos.* **2020**, *107*, 103499. [CrossRef]
8. Sharif, A.M.; Assi, N.A.; Al-Osta, M.A. Use of UHPC slab for continuous composite steel-concrete girders. *Steel Compos. Struct.* **2020**, *34*, 321–332. [CrossRef]
9. Wu, Z.; Shi, C.; Khayat, K.H. Investigation of mechanical properties and shrinkage of ultra-high performance concrete: Influence of steel fiber content and shape. *Compos. Part B Eng.* **2019**, *174*, 107021. [CrossRef]
10. Zhou, Z.; Qiao, P. Durability of ultra-high performance concrete in tension under cold weather conditions. *Cem. Concr. Compos.* **2018**, *94*, 94–106. [CrossRef]
11. Shi, Y.; Long, G.; Ma, C.; Xie, Y.; He, J. Design and preparation of ultra-high performance concrete with low environmental impact. *J. Clean. Prod.* **2019**, *214*, 633–643. [CrossRef]
12. Ganesh, P.; Murthy, A.R. Tensile behaviour and durability aspects of sustainable ultra-high performance concrete incorporated with GGBS as cementitious material. *Constr. Build. Mater.* **2019**, *197*, 667–680. [CrossRef]
13. Vincler, J.P.; Sanchez, T.; Turgeon, V.; Conciatori, D.; Sorelli, L. A modified accelerated chloride migration tests for UHPC and UHPFRC with PVA and steel fibers. *Cem. Concr. Res.* **2019**, *117*, 38–44. [CrossRef]
14. Zhu, J.-S.; Wang, Y.; Yan, J.-B.; Guo, X.-Y. Shear behaviour of steel-UHPC composite beams in waffle bridge deck. *Compos. Struct.* **2020**, *234*, 111678. [CrossRef]
15. Zhang, X.; Li, X.; Liu, R.; Hao, C.; Cao, Z. Dynamic properties of a steel–UHPC composite deck with large U-ribs: Experimental measurement and numerical analysis. *Eng. Struct.* **2020**, *213*, 110569. [CrossRef]
16. Zhu, Y.; Zhang, Y.; Hussein, H.H.; Chen, G. Flexural strengthening of reinforced concrete beams or slabs using ultra-high performance concrete (UHPC): A state of the art review. *Eng. Struct.* **2020**, *205*, 110035. [CrossRef]
17. Farzad, M.; Sadeghnejad, A.; Rastkar, S.; Moshkforoush, A.; Azizinamini, A. A theoretical analysis of mechanical and durability enhancement of circular reinforced concrete columns repaired with UHPC. *Eng. Struct.* **2020**, *209*, 109928. [CrossRef]
18. Ragalwar, K.; Heard, W.F.; Williams, B.A.; Ranade, R. Significance of the particle size distribution modulus for strain-hardening-ultra-high performance concrete (SH-UHPC) matrix design. *Constr. Build. Mater.* **2020**, *234*, 117423. [CrossRef]
19. Norhasri, M.M.; Hamidah, M.; Fadzil, A.M. Inclusion of nano metaclayed as additive in ultra high performance concrete (UHPC). *Constr. Build. Mater.* **2019**, *201*, 590–598. [CrossRef]
20. Arora, A.; Almujaddidi, A.; Kianmofrad, F.; Mobasher, B.; Neithalath, N. Material design of economical ultra-high performance concrete (UHPC) and evaluation of their properties. *Cem. Concr. Compos.* **2019**, *104*, 103346. [CrossRef]

21. Sadrmomtazi, A.; Tajasosi, S.; Tahmouresi, B. Effect of materials proportion on rheology and mechanical strength and microstructure of ultra-high performance concrete (UHPC). *Constr. Build. Mater.* **2018**, *187*, 1103–1112. [CrossRef]
22. Shi, C.; Wu, Z.; Xiao, J.; Wang, D.; Huang, Z.; Fang, Z. A review on ultra high performance concrete: Part I. Raw materials and mixture design. *Constr. Build. Mater.* **2015**, *101*, 741–751. [CrossRef]
23. Sohail, M.G.; Wang, B.; Jain, A.; Kahraman, R.; Ozerkan, N.G.; Gencturk, B.; Dawood, M.; Belarbi, A. Advancements in Concrete Mix Designs: High-Performance and Ultrahigh-Performance Concretes from 1970 to 2016. *J. Mater. Civ. Eng.* **2018**, *30*, 04017310. [CrossRef]
24. Chen, X.; Wan, D.-W.; Jin, L.-Z.; Qian, K.; Fu, F. Experimental studies and microstructure analysis for ultra high-performance reactive powder concrete. *Constr. Build. Mater.* **2019**, *229*, 116924. [CrossRef]
25. Yang, R.; Yu, R.; Shui, Z.; Gao, X.; Han, J.; Lin, G.; Qian, D.; Liu, Z.; He, Y. Environmental and economical friendly ultra-high performance-concrete incorporating appropriate quarry-stone powders. *J. Clean. Prod.* **2020**, *260*, 121112. [CrossRef]
26. Dong, Y. Performance assessment and design of ultra-high performance concrete (UHPC) structures incorporating life-cycle cost and environmental impacts. *Constr. Build. Mater.* **2018**, *167*, 414–425. [CrossRef]
27. Zhang, X.; Liu, Z.; Wang, F. Autogenous shrinkage behavior of ultra-high performance concrete. *Constr. Build. Mater.* **2019**, *226*, 459–468. [CrossRef]
28. Qian, D.; Yu, R.; Shui, Z.; Sun, Y.; Jiang, C.; Zhou, F.; Ding, M.; Tong, X.; He, Y. A novel development of green ultra-high performance concrete (UHPC) based on appropriate application of recycled cementitious material. *J. Clean. Prod.* **2020**, *261*, 121231. [CrossRef]
29. Zhang, X.; Zhao, S.; Liu, Z.; Wang, F. Utilization of steel slag in ultra-high performance concrete with enhanced eco-friendliness. *Constr. Build. Mater.* **2019**, *214*, 28–36. [CrossRef]
30. Zhang, H.; Ji, T.; He, B.; He, L. Performance of ultra-high performance concrete (UHPC) with cement partially replaced by ground granite powder (GGP) under different curing conditions. *Constr. Build. Mater.* **2019**, *213*, 469–482. [CrossRef]
31. Yang, R.; Yu, R.; Shui, Z.; Guo, C.; Wu, S.; Gao, X.; Peng, S. The physical and chemical impact of manufactured sand as a partial replacement material in Ultra-High Performance Concrete (UHPC). *Cem. Concr. Compos.* **2019**, *99*, 203–213. [CrossRef]
32. Visage, E.T.; Weldon, B.D.; Jauregui, D.V.; Newtson, C.M. Flexural Performance of Ultrahigh-Performance Concrete Developed Using Local Materials. *J. Mater. Civ. Eng.* **2019**, *31*, 04019050. [CrossRef]
33. Ma, R.; Guo, L.; Sun, W.; Liu, J.; Zong, J. Strength-enhanced ecological ultra-high performance fibre-reinforced cementitious composites with nano-silica. *Mater. Struct.* **2017**, *50*, 166. [CrossRef]
34. Ma, R.; Guo, L.; Ye, S.; Sun, W.; Liu, J. Influence of Hybrid Fiber Reinforcement on Mechanical Properties and Autogenous Shrinkage of an Ecological UHPFRCC. *J. Mater. Civ. Eng.* **2019**, *31*, 04019032. [CrossRef]
35. Yang, R.; Yu, R.; Shui, Z.; Gao, X.; Xiao, X.; Zhang, X.; Wang, Y.; He, Y. Low carbon design of an Ultra-High Performance Concrete (UHPC) incorporating phosphorous slag. *J. Clean. Prod.* **2019**, *240*, 118157. [CrossRef]
36. Li, P.; Cao, Y.; Brouwers, H.; Chen, W.; Yu, Q. Development and properties evaluation of sustainable ultra-high performance pastes with quaternary blends. *J. Clean. Prod.* **2019**, *240*, 118124. [CrossRef]
37. Bae, Y.; Pyo, S. Ultra high performance concrete (UHPC) sleeper: Structural design and performance. *Eng. Struct.* **2020**, *210*, 110374. [CrossRef]
38. Zhou, M.; Lu, W.; Song, J.; Lee, G.C. Application of Ultra-High Performance Concrete in bridge engineering. *Constr. Build. Mater.* **2018**, *186*, 1256–1267. [CrossRef]
39. Abdelbaset, H.; Cheng, B.; Tian, L.; Li, H.-T.; Zhang, Q.-H. Reduce hot spot stresses in welded connections of orthotropic steel bridge decks by using UHPC layer: Experimental and numerical investigation. *Eng. Struct.* **2020**, *220*, 110988. [CrossRef]
40. Shao, X.; Deng, L.; Cao, J. Innovative steel-UHPC composite bridge girders for long-span bridges. *Front. Struct. Civ. Eng.* **2019**, *13*, 981–989. [CrossRef]
41. Zhou, Z.; Qiao, P. Tensile behavior of ultra-high performance concrete: Analytical model and experimental validation. *Constr. Build. Mater.* **2019**, *201*, 842–851. [CrossRef]
42. Richard, P.; Cheyrezy, M.H. Reactive Powder Concretes with High Ductility and 200–800 Mpa Compressive Strength. *Special Publication-R. Soc. Chem.* **1994**, *144*, 507–518. [CrossRef]
43. Yu, R.; Spiesz, P.; Brouwers, H. Development of an eco-friendly Ultra-High Performance Concrete (UHPC) with efficient cement and mineral admixtures uses. *Cem. Concr. Compos.* **2015**, *55*, 383–394. [CrossRef]
44. Li, P.; Yu, Q.; Brouwers, H. Effect of coarse basalt aggregates on the properties of Ultra-high Performance Concrete (UHPC). *Constr. Build. Mater.* **2018**, *170*, 649–659. [CrossRef]
45. Wu, Z.; Khayat, K.H.; Shi, C. Changes in rheology and mechanical properties of ultra-high performance concrete with silica fume content. *Cem. Concr. Res.* **2019**, *123*, 105786. [CrossRef]
46. Žurauskienė, R.; Valentukevičienė, M. Experimental Research on Quality Parameters of Recycled Concrete. *Materials* **2020**, *13*, 2538. [CrossRef]
47. Zhong, R.; Wille, K.; Viegas, R. Material efficiency in the design of UHPC paste from a life cycle point of view. *Constr. Build. Mater.* **2018**, *160*, 505–513. [CrossRef]
48. Sbia, L.A.; Peyvandi, A.; Lu, J.; Abideen, S.; Weerasiri, R.R.; Balachandra, A.M.; Soroushian, P. Production methods for reliable construction of ultra-high-performance concrete (UHPC) structures. *Mater. Struct.* **2017**, *50*, 7. [CrossRef]

49. Xu, Y.; Jin, R.; Hu, L.; Li, B.; Chen, W.; Shen, J.; Wu, P.; Fang, J. Studying the mix design and investigating the photocatalytic performance of pervious concrete containing TiO2-Soaked recycled aggregates. *J. Clean. Prod.* **2019**, *248*, 119281. [CrossRef]
50. Guo, L.; Wu, J.; Wang, H. Mechanical and perceptual characterization of ultra-high-performance cement-based composites with silane-treated graphene nano-platelets. *Constr. Build. Mater.* **2020**, *240*, 117926. [CrossRef]
51. Wu, J.-D.; Guo, L.-P.; Cao, Y.-Z.; Lyu, B.-C. Mechanical and fiber/matrix interfacial behavior of ultra-high-strength and high-ductility cementitious composites incorporating waste glass powder. *Cem. Concr. Compos.* **2022**, *126*, 104371. [CrossRef]
52. Deboucha, W.; Leklou, N.; Khelidj, A.; Oudjit, M.N. Hydration development of mineral additives blended cement using thermogravimetric analysis (TGA): Methodology of calculating the degree of hydration. *Constr. Build. Mater.* **2017**, *146*, 687–701. [CrossRef]